JOURNAL OF MULTIFUNCTIONAL MATERIALS & PHOTOSCIENCE
7(2), December 2016, pp. 81-97

A review on CVD products based materials for supercapacitor electrodes

Shu Ye, Won-Chun Oh[1*]

Department of Advanced Materials Science & Engineering, Hanseo University, Seosan-si, Chungnam, Korea, 356-706

Abstract: The carbon materials are promising for applications in supercapacitors and other energy storage devices due to the intriguing properties, highly tunable surface area, outstanding electrical conductivity, good chemical stability and excellent mechanical behavior. This review summarizes our recent development on carbon materials for supercapacitor electrodes obtained by chemical vapor deposition (CVD) method. This series of CVD products include graphene-carbon nanotubes (G-CNT) growth on Cu foil, Carbon nanotubes growth on chemically synthesized graphene (CG-CNT) and carbon nanotubes growth on activated carbon (G-AC). There are extensive and on-going researches on the rationalization of their structures at varying scales and dimensions, development of effective and low cost synthesis techniques, design and architecting of carbon-based materials, as well as clarification of their electrochemical performance. It is indicated that future studies should focus on the overall device performance in energy storage devices and large-scale process in low costs for the promising applications in portable and wearable electronic, transport, electrical and hybrid vehicles.

Keywords: Carbon materials; CVD; Supercapacitors; EDLC

1. Introduction

Supercapacitors or ultracapacitors have attracted considerable recent attentions due to their high power density, high charge/discharge rates, and long cycle life performance[1], [2] and [3]. They are considered as one of the most promising electrochemical energy storage devices, having a potential to complement or eventually replace the batteries for energy storage applications, i.e., those for wearable and portable electronic, electrical and hybrid vehicles [4-8]. Based on the energy storage mechanisms, supercapacitors can be classified into to two main categories, i.e., electric double layer capacitors (EDLCs) and pseudo capacitors [9-13]. For EDLCs, the capacitance is originated from the accumulation of charges at the electrode-electrolyte interfaces. Therefore, controlling the specific surface area and pore size and enhancing electrical conductivity are the effective ways to achieve a high storage capacity [14-15]. Also, the energy storage of pseudo capacitance is realized through transferring the faradic charges between

*Corresponding author: *wc_oh@hanseo.ac.kr*

electrolyte and electrode due to the reversible multi-electron redox faradaic reactions, which generally exhibits higher specific capacitance and energy density, compared to EDLCs [16-19]. However, the poor electrical conductivity in the commonly known pseudo capacitive electrodes can restrict the Faradic reactions, therefore leading to unsatisfactory electrochemical performance and life cycles.

Chemical vapor deposition (CVD) over transition metals have attracted a great interest as an effective and powerful means to prepare easily-transferrable, high quality graphene films [20]. However, the thermal CVD process involves high growth temperature and catalytic ability of metals can have only limited applications in coating technology [21]. In these prospects, a one-step low temperature CVD technique to deposit large-area graphene coating can be extremely suitable for industrial application and can pave the way for direct coating on various substrates.

In this review, our new CVD technique, resultant structures and electrochemical performance of graphene-based materials designed for applications in supercapacitors was summarized. Coin-type EDLC cells with two symmetrical carbon electrode were assembled using the CVD products. Electrochemical performance of the carbon electrodes was measured by galvanostatic charge/discharge and cyclic voltammetry methods.

2. CVD growth of G-CNTÿCG-CNT and AC-CNT

Benzene used as a carbon precursor material was purchased from Dae-Jung Chemical and Metals Co. Ltd Korea. Argon and Nitrogen gas were purchased from Samchun Pure Chemical Co. Ltd., Korea. A specially designed split Si tube furnace divided into two parts, the inner tube and the outer tube, was used. The dimensions of the tube are 30 cm length and 4 cm outer diameter, with two nozzles, one for the inlet of benzene vapors and the other for the inlet of Ar and N_2 gas. The inner furnace, also called the growth zone (Fig. 1a), having a 5cm length and 4 cm diameter, is used to grow the CNT on AC. The

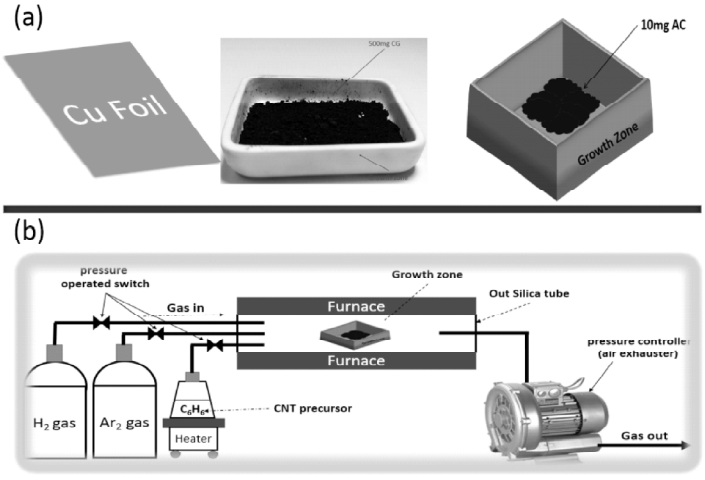

Figure 1: Schematic of CVD products on Cu foil, chemically synthesized graphene and activated carbon [22]

benzene was first heated below its boiling temperature and vapors were produced. The vapors were then transferred to the tube simultaneously with Ar gas which also acts as a carrier for benzene vapors. The vapor flow and the Ar gas ratio were controlled through the control valve. The furnace temperature was increased to corresponding temperature at the first step and Ar/H_2 gas was released into the Si furnace, then the growth zone was inserted in the inner tube followed by controlled amount of Ar/H_2 gas and benzene vapors. The growth of CVD product was checked at corresponding time and tempereture. Fig. 1b shows a typical G-AC growth process.

3. Morphological characterization of CVD products.

The FESEM images of the G-CNTs are shown in Fig 2(a-b). In Fig. 2 (a) the small dots can be seen very clearly spotted white in color. These dots are further responsible for the CNTs concentric graphene sheet rolling into a tube format. In Fig. 2(b), the CNTs on the Cu substrate are clearly visible in tube type shape. The densities of CNTs are quite large so that graphene layers are not visible in the image. These formed CNTs are found to vertical on graphene sheet which are confirmed from Raman (Fig. 4). Our observation further shows that by controlling a number of experimental parameters, these CNTs can be grown in a convenient manner on a graphene sheet, which may be beneficial point for future graphene based nanoelectronics devices [33-35].

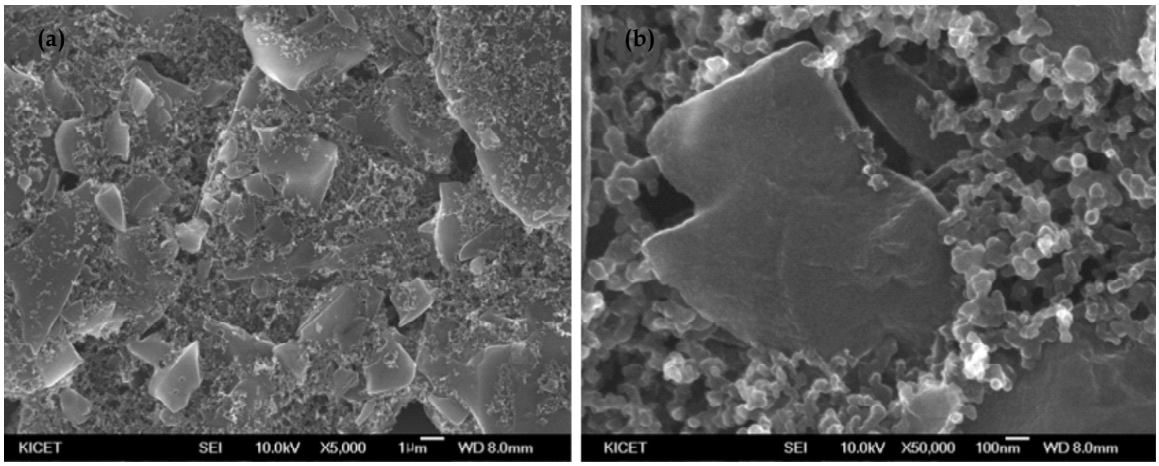

Figure 2: FESEM images of the as-prepared G-CNT sample under 8 minute reaction time: (a) X 50,000, and (b) X 100,000 [23]

Fig. 3. show TEM images of as-prepared samples. The two-dimensional structure of the graphene sheet is clearly shown to have been retained with partial agglomeration in Fig. 3(a). The TEM image in Fig. 3(b) further confirms the tip type CNTs which is closed from the outer end. Here, we can observe that the circular CNTs wound together in bundle type shapes. This means that at the edges of large area graphene, CNTs were grown and the density reduces at the interior of the sheet. These results give us new insight into G-CNTs composites. The edge CNTs may be very helpful to develop ultrafast nanoelectronics devices by providing sharp anchoring sites.

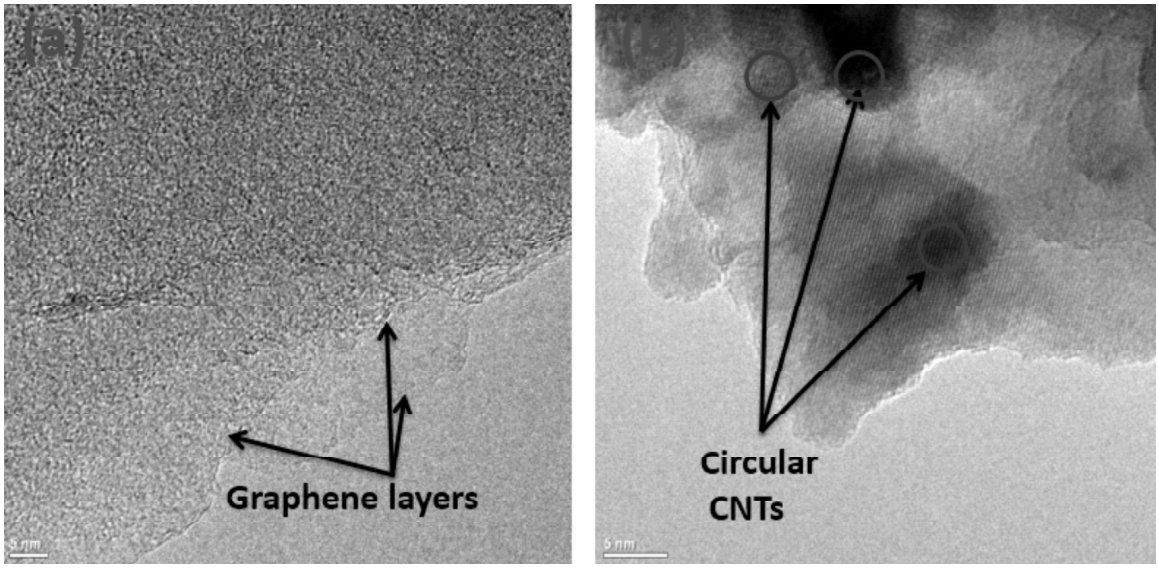

Figure 3: HRTEM images of G-CNT growth on Cu foil [24]

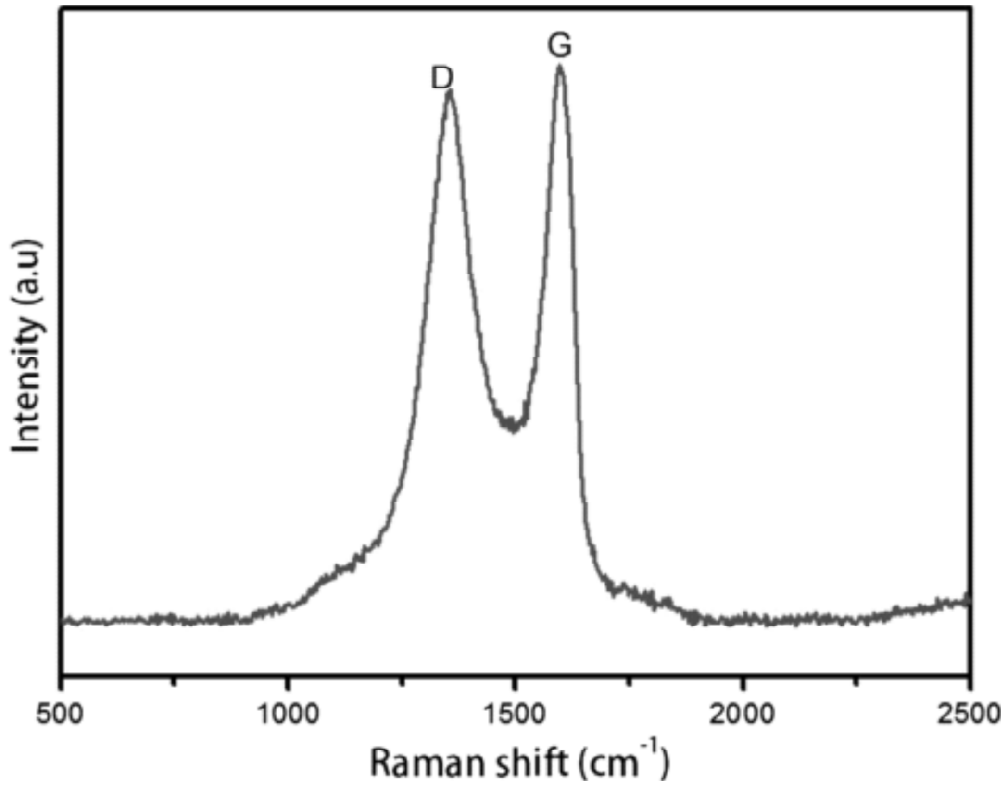

Figure 4: Raman spectra of G-CNT powder [25]

Raman spectroscopy is a useful technique to study the structure and electronic properties of carbon materials such as graphene/graphite and carbon nanotubes. Fig. 4 describes the Raman spectra of the G-CNTs powder. The variation in the Raman band intensity and the shift provides information on the nature of the C–C bonds and defects. The Raman spectra in Fig. 4 shows the characteristic D and G bands at 1354 and 1590 cm^{-1}, respectively, that are found in graphene. The D band is a common feature for sp^3 defects in carbon, and the G band provides information on the in-plane vibrations of the sp^2 bonded carbons [26-27]. The intensity ratio of the D band to the G band usually reflects the order of the defects in G-CNTs.

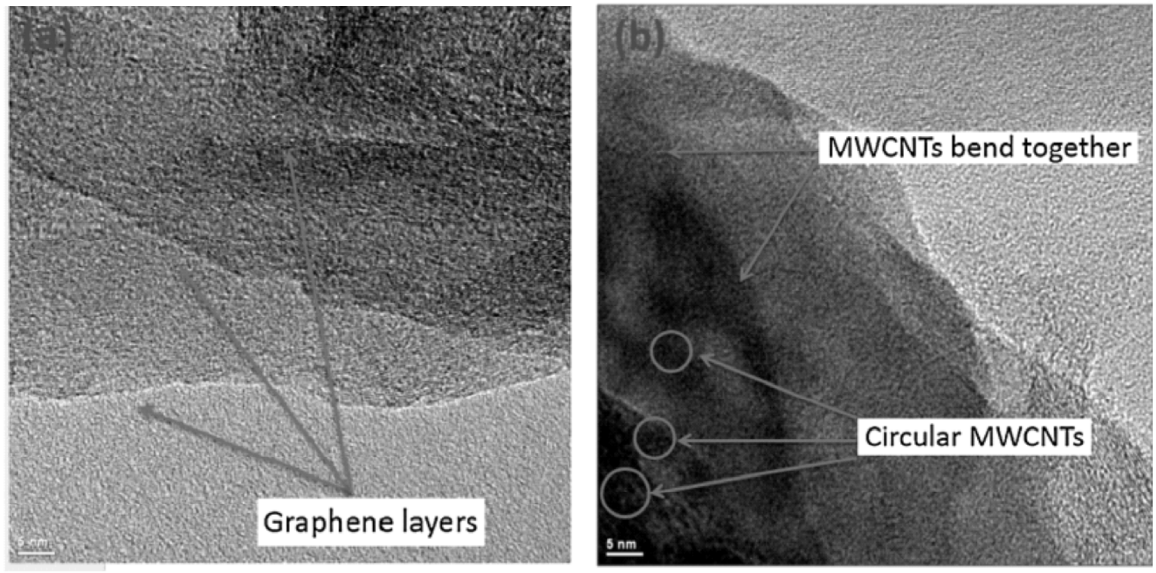

Figure 5: SEM images of the as-prepared CNT-CG sample under 30 minute reaction [28]

Fig. 5 shows the SEM image of the CNT-CG, clearly illustrating the growth of the CNTs on the CG and the relatively large densities of the CNTs. These formed CNTs are

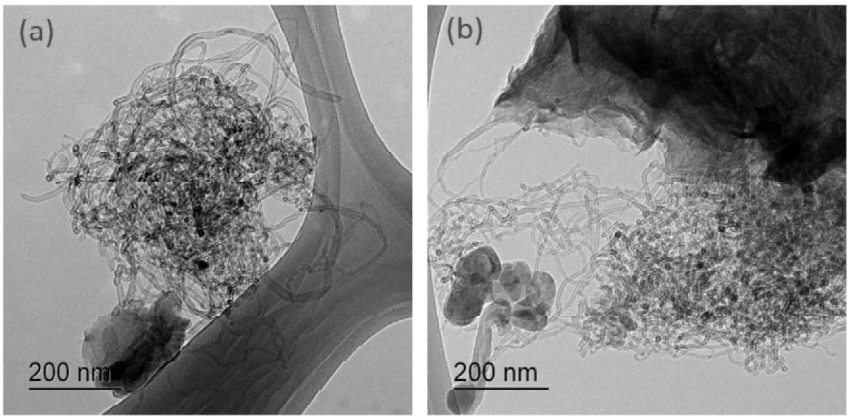

Figure 6: TEM images of CNT-CG: (a) 1 μm; (b) 200 nm [32]

found to lie vertical on the graphene sheet. We further observed that by controlling a number of experimental parameters, these CNTs can be grown in a convenient manner on a graphene sheet, which could be beneficial for future graphene-based nano electronics devices [29-31].

The TEM image in Fig. 6 further confirms the type of tip of the CNTs, which are closed from the outer end. Here, we can observe that the circular CNTs are wound together in bundles. This means that CNTs grew at the edges of CG, and the density reduced at the interior of the sheet. These results give us new insight into CNT-CG composites. The edge CNTs could be very helpful for developing ultrafast nano electronic devices, by providing sharp anchoring sites.

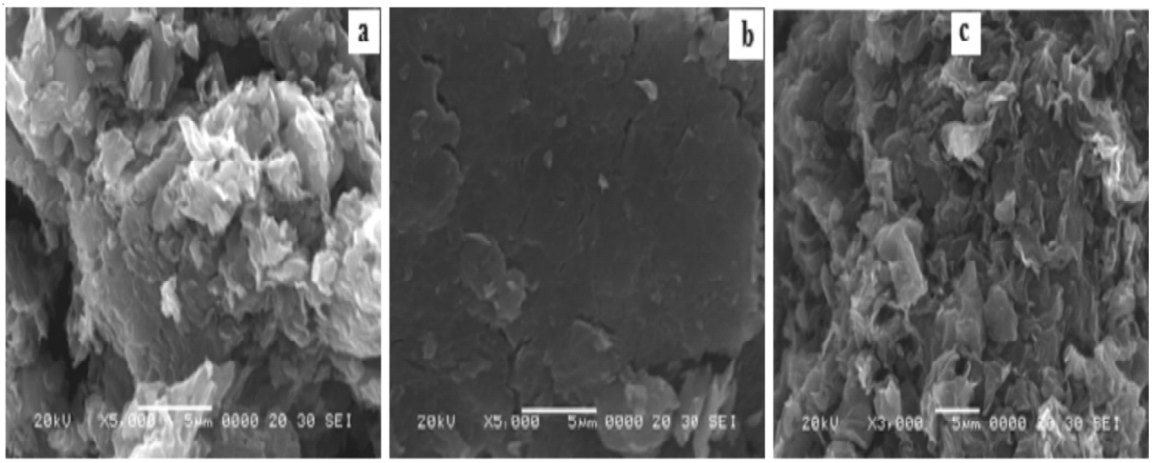

Figure 6: SEM image of graphene/activated carbon composite [33]

The SEM images of the G-AC are shown in Fig. 6. This formed graphene are found to vertical on activated carbon which are confirmed from Raman (Fig. 7). Our observation further shows that by controlling a number of experimental parameters, It is observed that graphen surface is crumpled with some wrinkles suggesting that some pores pf the micrometer rangre were present.[34-35].

Raman spectroscopy is a useful technique to study the structure and electronic properties of carbon materials such as graphene/graphite and carbon nanotubes. Fig. 7 describes the Raman spectra of the G-AC powder. The variation in the Raman band intensity and the shift provides information on the nature of the C–C bonds and defects. Fig. 7 shows the characteristic D and G bands at 1349 and 1577 cm^{-1}, respectively, that are found in CNTs. The D band is a common feature for sp^3 defects in carbon, and the G band provides information on the in-plane vibrations of the sp^2 bonded carbons [15-21]. The intensity ratio of the D band to the G band usually reflects the order of the defects in G-AC.

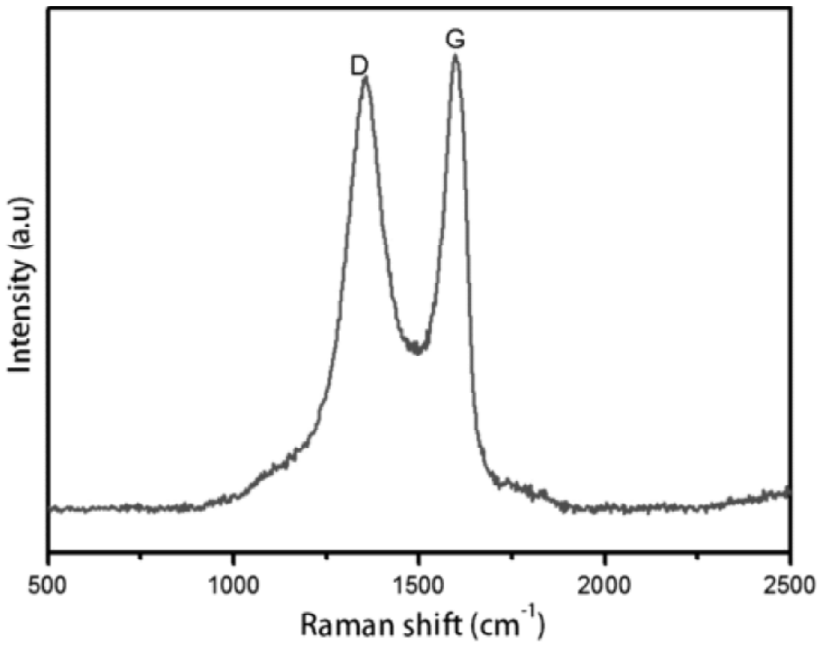

Figure 7: Raman spectra of G-ACpowder [36].

4. Fabrication of CVD products based electrodes

Table 1
Parameters of electrode composition with G-CNT, AC, and PTFE [37]

Sample name	*Active material* YP50F	*Additive material* G-CNT	*Conductive Material*	*Binder*	*Electrode size*
G-CNT6	MSP20 (79)	G-CNT (6)	SPB (8)	PTFE (7)	2.5 × 2.5 cm
G-CNT8	MSP20 (77)	G-CNT (8)	SPB (8)	PTFE (7)	
G-CNT10	MSP20 (75)	G-CNT (10)	SPB (8)	PTFE (7)	

Table 2
Parameters of electrode composition with CG-CNT, AC, and PTFE [38]

Sample name	*Active material YP50F*	*Additive material CG-CNT*	*Conductive Material*	*Binder*	*Electrode size*
YCG6	YP50F (79)	CG-CNT (6)	SPB (8)	PTFE (7)	2.5 × 2.5 cm
YCG8	YP50F (77)	CG-CNT (8)	SPB (8)	PTFE (7)	
YCG10	YP50F (75)	CG-CNT (10)	SPB (8)	PTFE (7)	

Table 3
Parameters of electrode composition with G-AC, AC, and PTFE [39]

Sample name	*Active material YP50F*	*Additive material G-AC*	*Conductive Material*	*Binder*	*Electrode size*
GF1	YP50F (79)	G-AC (6)	SPB (8)	PTFE (7)	2.5 × 2.5 cm
GF2	YP50F (77)	G-AC	SPB (8)	PTFE (7)	
GF3	YP50F (75)	G-AC (10)	SPB (8)	PTFE (7)	

The fabrication of working electrodes was carried out as following and listed in Table 1. The electrodes were composed of CVD products based active carbon (MSP20 or YP50F) as an active material, Super-P carbon black (SPB) as a conductive material and PTFE based a mixed binder. The weight ratio of CVD products as an additional material was 6, 8 and 10 wt.%. In the electrodes, the mixed binder abbreviated as PTFE is consist of styrene-butadiene rubber (SBR), sodium salt of carboxymethyl cellulose (CMC), polytetrafluoroethylene ((C_2F_4), PTFE).

5. The measurement of EDLC Performance

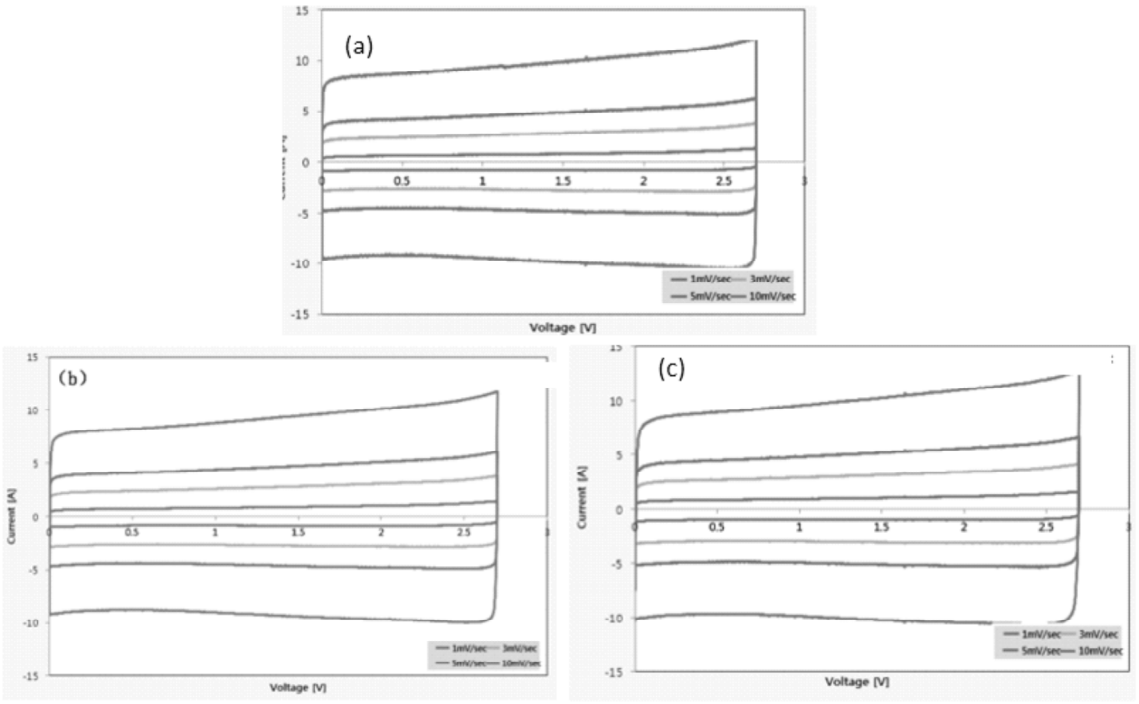

Figure 7: C-V curves of the as-prepared supercapacitors: (a): G-CNT6, (b) G-CNT8, (c): G-CNT10 [40]

To measure the electrochemical performance of the samples, cyclic voltammetry measurements were carried out from 0 – 2.75 V at various scan rates from 1–20 mV/s. Fig. 7, Fig8 and Fig. 9 shows the CV curve for each sample at different scan rates respectively. From the cyclic voltamogram, a rectangular curve is clearly evident for all scan rates, which indicates the electrical double layer capacitor of the electrode material, with no pseudo capacitance effect due to functional groups. The specific capacitance measured from the rectangular CV curves was at a scanning rate of 1–20 mV/s between 0–2.75 V.

Fig. 10 shows the specific capacitance for 40,60 and100 cycles at a current density from 0.1 mA cm^{-2} to 50 mA cm^{-2}. The devices exhibited excellent stability and reliability at high current charge/discharge cycles. The high stability of the supercapacitors at different

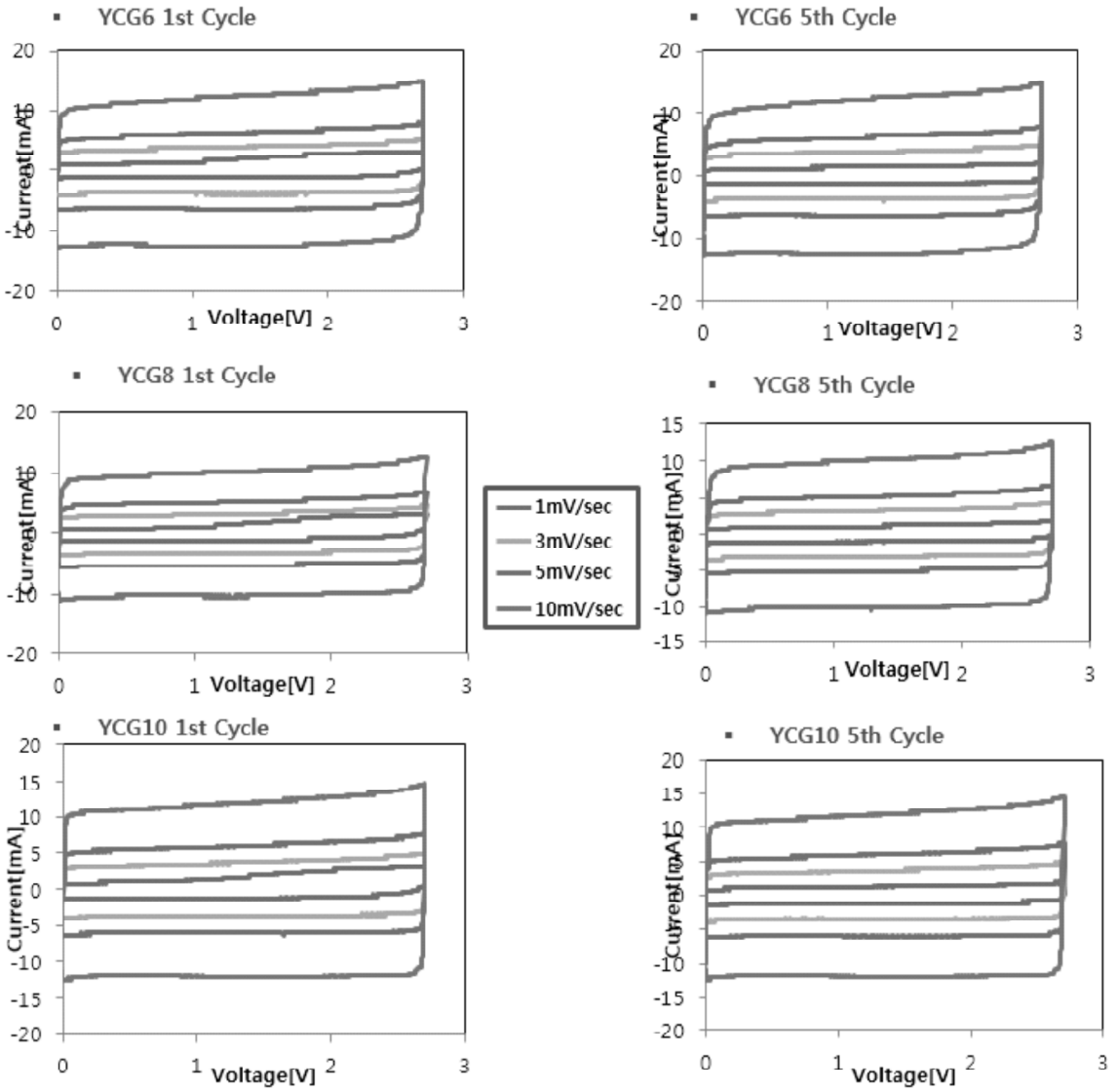

Figure 8: CV curves of MEG serial electrodes for the 5th test at different scan rates of 1, 3, 5, and 10 mV/s [41]

densities suggests that these energy storage devices are suitable for fast charging applications. The cycling performance of G-CNT8 electrode was excellent; it indicates that the CVD products material really enhanced the specific capacitance of as-prepared samples. From Fig. 11, during the cycle experiments by applying voltage across the capacitor the values of the charge/discharge cycles remain almost the same for all samples. These result further confirm that stability of our prepared EDLCs.

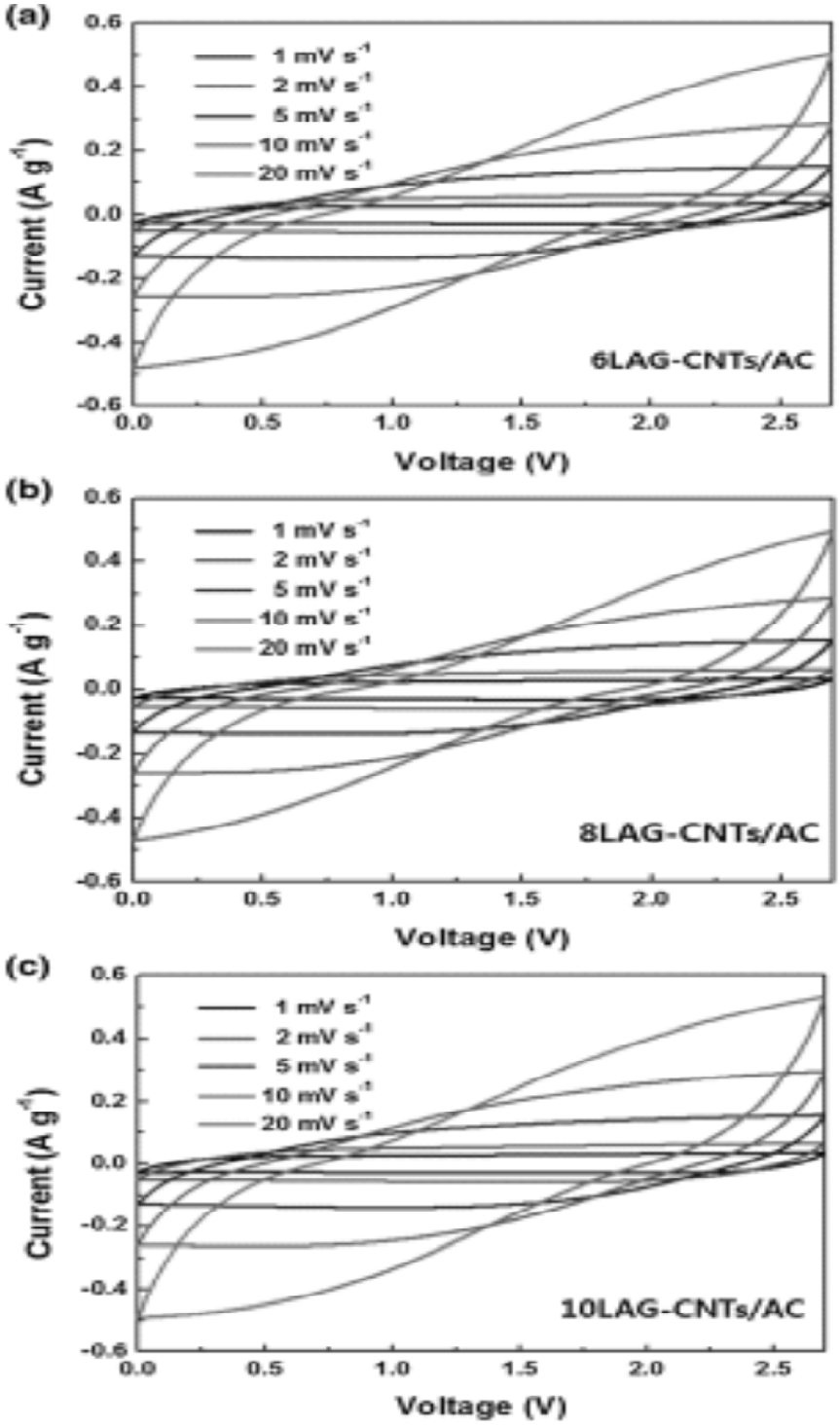

Figure 9: C-V curves of as-prepared supercapacitors; (a): YP50F, (b): G-AC6, (c): G-AC8, (d): G-AC10 [42]

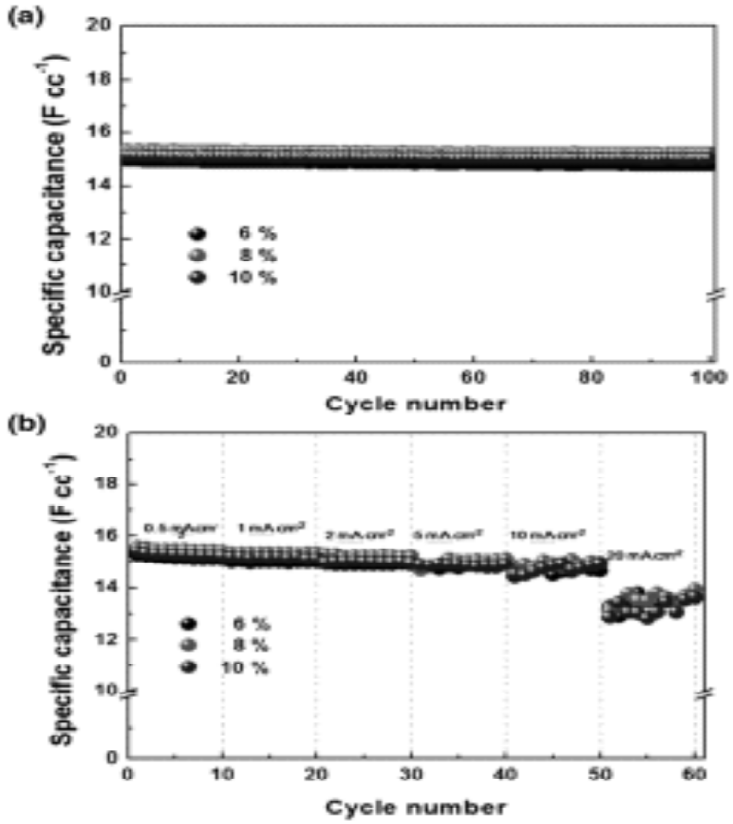

Figure 10: Cycle performance of the as-prepared samples [43]

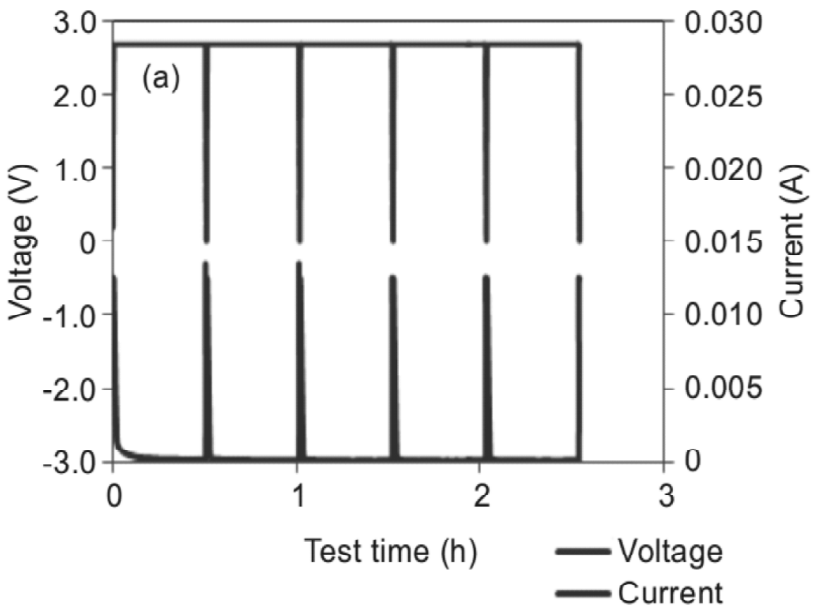

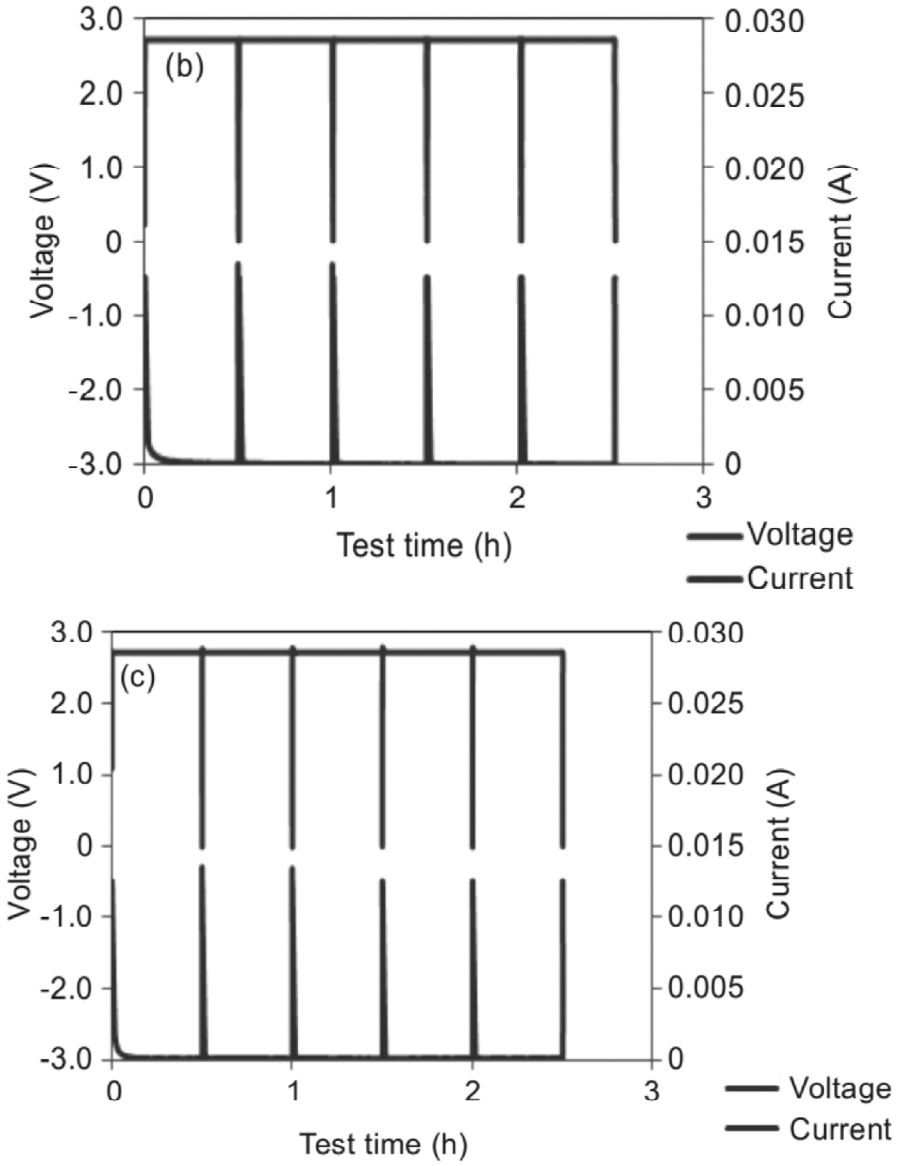

Figure 11: Charge discharge profile of the GF1, GF2 and GF3 [44-45]

Fig. 12, Fig.13 and Fig. 14 presents the Nyquist plots of the CVD products based capacitor cells with different weight ratios of CVD products in their carbonaceous electrodes with fixed PTFE. All electrode coatings had a thickness of 199–205 μm, whereas the standard activated carbon fiber electrode had a thickness of 20 μm. The smaller thickness of the AC electrode substantially reduces the resistance [49]. The measurements of electrochemical impedance spec-troscopy on the cells were carried out at sinusoidal

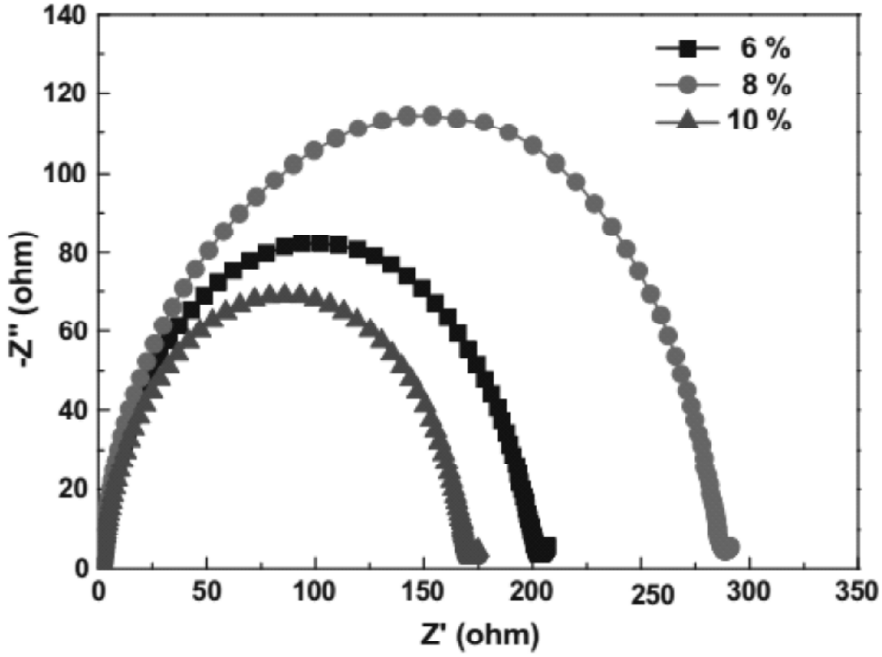

Figure 12: Electrochemical impedance spectra of the as-prepared samples: (a): G-CNT6, (b) G-CNT8, (c): G-CNT10 [46].

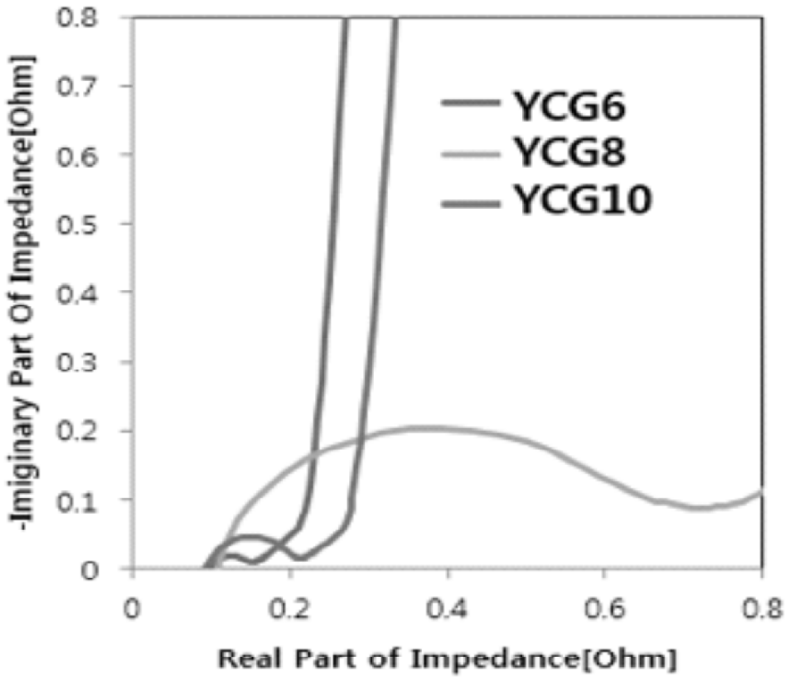

Figure 13: Electrochemical impedance spectra of the as-prepared samples [47]

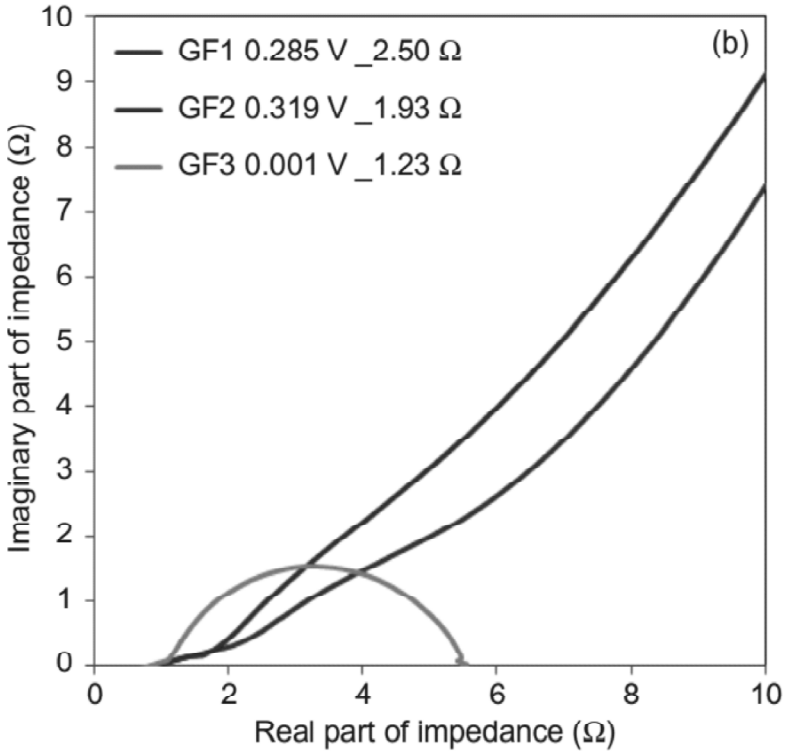

Figure 14: Nyquist plot of G-AC based EDLCs [48].

signal of 5 mV over a frequency range from 100 mHZ to 100 KHz. From the Nyquist plot, R_s and R_{ct}, could be instantly determined, which are the solution resistance and charge transfer resistances, respectively. The former comes from the bulk solution, and its magnitude depends upon the material used, and thickness and conduc-tivity of the electrolyte. R_{ct} can be divided into two parts, elec-tronic and ionic resistance [50]. The electronic resistance includes the inherent electronic conductivity of the carbon particles, the interaction between the particles, and the contact between layers of EDLCs. The ionic resistance depends on the porous texture and thickness of the active layers. The semicircle comes from the parallel RC branch. From this plot, R_{int} can be determined between the low frequency region on the X-axis and the straight section of the plot [51].

The capacitance can be estimated by:

$C = 1/2\pi fZim$

The Nyquist plots show that the semicircle decreased with decreasing value of CVD products in the sample, while the R_s remains unchanged. This indicates that the decreasing graphene value in the cell can reduce the charge transfer resistance, and has little effect on the solution resistance. Another reason for the improvement is the incorporation of CVD products and PTFE in the pores of the activated carbon to increase the conductivity, and enhance the contact between the EDLC layers. This decrease in R_{ct} indicates the optimum

loading of graphene in EDLCs. It is also evidence of the decrease in porosity, which further decreases the capacitance [52-55].

The Nyquist plot clearly indicates that the G-CNT6, YCG8 and GF3 EDLC has the smallest charge transfer resistance among the other composites in the series.

4. Conclusion and outlook

CVD products in different forms have proven to be excellent candidates of electrode materials in electrochemical energy storage systems, such as supercapacitors. In recent years, considerable efforts have been made on the structural design, material fabrication, performance evaluation, as well as understanding of the key electrochemical phenomena observed. To realize the expected full-scale practical application, the quality and reproducible quantity of the electrode materials both will have to be further improved. CVD products based electrode materials with different architectures exhibit varying physical, mechanical and chemical behaviors, therefore affecting their performance in supercapacitor. More attention should be paid to further exploring the tunable 3D structure with interconnected porous structure, which can be manipulated for large internal surface area, ion/charge pathways, and avoiding the dead volume and collapse of the overall structures.

Reference

[1] R. Patrice, B. Gerand, J.B. Leriche, L. Seguin, E. Wang, R. Moses, K. Brandt, J.M. Tarascon, J. Electrochem. Soc. 148 (2001) 448.

[2] C.C. Yang, G.M. Wu, Mater. Chem. Phys. 114 (2009) 948–955.

[3] S. Biswas, L.T. Drzal, Chem. Mater. 22 (2010) 5667.

[4] S.C. Pang, M.A. Anderson, T.W. Chapman, J. Electrochem. Sci. 10 (2000) 444–450.

[5] R.N. Reddy, R.G. Reddy, J. Power Sources 124 (2003) 330–337.

[6] N.S.A. Aziz, T. Nishiyama, N.I. Rusli, M.R. Mahmood, K. Yasui, A.M. Hashim, Nanoscale Res. Lett. 9 (2014).

[7] N.S.A. Aziz, M.R. Mahmood, K. Yasui, A.M. Hashim, Nanoscale Res. Lett. 9 (2014).

[8] N.F. Ahmad, N.I. Rusli, M.R. Mahmood, K. Yasui, A.M. Hashim, Nanoscale Res. Lett. 9 (2014).

[9] Y. Zhang, Z. Xie, Z. Wang, X. Feng, Y. Wang, A. Wu, Dalton Trans. (2016).

[10] X. Li, Y. Zhu, W. Cai, M. Borysiak, B. Han, D. Chen, R.D. Piner, L. Colombo, R.S. Ruoff, Nano Lett. 9 (12) (2009) 4359–4363.

[11] X. Wang, S.M. Tabakman, H. Dai, J. Am. Chem. Soc. 130 (26) (2008) 8152–8153.

[12] J.R. Ostrick, A. Dodabalapur, L. Torsi, A.J. Lovinger, E.W. Kwock, T.M. Miller, M. Galvin, M. Berggren, H.E. Katz, J. Appl. Phys. 81 (10) (1997) 6804.

[13] A. Zaban, O.I. Micic, B.A. Gregg, A.J. Nozik, Langmuir 14 (11) (1998) 3153–3156.

[14] J. Qi, W. Liu, C. Biswas, G. Zhang, L. Sun, Z. Wang, X. Hu, Y. Zhang, Opt. Commun. 349 (2015) 198–202.

[15] Q. Shen, A. Yamada, S. Tamura, T. Toyoda, Appl. Phys. Lett. 97 (12) (2010) 4–7.

[16] I. Robel, V. Subramanian, M. Kuno, P.V. Kamat, J. Am. Chem. Soc. 128 (7) (2006) 2385–2393.

[17] X. Gao, H. Li, W. Sun, Q. Chen, F. Tang, L. Peng, J. Phys. Chem. C 113 (18) (2009) 7531–7535.

[18] C.H.M. Chuang, P.R. Brown, V. Bulović, M.G. Bawendi, Nat. Mater. 13 (2014) 1–6.

[19] X. Yao, Y. Chang, G. Li, L. Mi, S. Liu, H. Wang, Y. Yu, Y. Jiang, Sol. Energy Mater. Sol. Cells 137 (2015) 287–292.

[20] A.R. Marshall, M.R. Young, A.J. Nozik, M.C. Beard, J.M. Luther, J. Phys. Chem. Lett. 6 (2015) 2892–2899.

[21] H.K. Jun, M.A. Careem, A.K. Arof, Renew. Sust. Energy Rev. 22 (2013) 148–167.

[22] Q. Zhou, Z. Fang, J. Li, M. Wang, Microporous Mesoporous Mater. 202 (2015) 22–35.

[23] D. Chen, K. Wang, D. Xiang, R. Zong, W. Yao, Y. Zhu, Appl. Catal. B: Environ. 147 (2014) 554–561.

[24] P. Chandran, P. Kumari, S.S. Khan, Sol. Energy 105 (2014) 542–547.

[25] O. Bechambi, A. Touati, S. Sayadi, W. Najjar, Mater .Sci. Semicond. Process. 39 (2015) 807–816.

[26] J.Z. Bloh, A. Folli, D.E. Macphee, J. Phys. Chem. C 118 (2014) 21281–21292.

[27] B.M. Pirzada, N.A. Mir, N. Qutub, O. Mehraj, S. Sabir, M. Muneer, Mater. Sci. Eng. B 193 (2015) 137–145.

[28] Y. Yang, L. Luo, M. Xiao, H. Li, X. Pan, F. Jiang, Mater. Sci. Semicond. Process. 40 (2015) 183–193.

[29] N. Boonprakob, N. Wetchakun, S. Phanichphant, D. Waxler, P. Sherrell, J. Colloid Interfac Sci. 417 (2014) 402–409.

[30] H. Yu, B. Xue, P. Liu, J. Qiu, W. Wen, S. Zhang, H. Zhao, ACS Appl. Mater. Interfaces 4 (2012) 1289–1294.

[31] Y. Zhang, J. Zhang, Q. Xu, S. Yan, S. Zhao, G. Luo, C. Li, Mater. Res. Bull. 53 (2014) 107–115.

[32] Y. Zhang, H. Xu, Y. Xu, H. Zhang, Y. Wang, J. Photochem. Photobiol. A 170 (2005) 279–285.

[33] S. Zhang, Z. Zheng, J. Wang, J. Chen, Chemosphere 65 (2006) 2282–2288.

[34] D.M. Tobaldi, R.C. Pullar, A.S. Škapin, M.P. Seabra, J.A. Labrincha, Mater. Res. Bull. 50 (2014) 183–190.

[35] H. Dang, V. Singh, S. Rajaputra, S. Guduru, J. Chen, B. Nadimpally, Sol. Energy Mater. Sol. Cells 126 (2014) 184–191.

[36] N.D. Sankir, B. Dogan, J. Mater. Process. Technol. 211 (3) (2011) 382–387.

[37] K. Heo, H. Lee, Y. Park, J. Park, H.J. Lim, D. Yoon, C. Lee, M. Kim, H. Cheong, J. Park, J. Jian, S. Hong, J. Mater. Chem. 22 (5) (2012) 2173.

[38] C. Ma, Q. Tang, D. Liu, Z. Zhao, B. He, H. Chen, L. Yu, J. Power Sources 276 (2015) 215–221.

[39] C.D. Lokhande, B.R. Ssnkapal, H.M. Pathan, M. Muller, M. Giersing, H. Tributsh, Appl. Surf. Sci. 181 (2001) 277–282.

[40] K.I. Ishibashi, Y. Kimura, M. Niwano, J. Appl. Phys. 103 (2008) 094507.

[41] A. Zaban, M. Greenshtein, J. Bisquert, Chem. Phys. Chem. 4 (2003) 859–864.

[42] P.R.F. Barnes, K. Miettunen, X. Li, A.Y. Anderson, T. Bessho, M. Gratzel, B. C. O'Regan, Adv. Mater. 25 (13) (2013) 1881–1922.

[43] G. Boschloo, A. Hagfeldt, J. Phys. Chem. B 109 (2005) 12093–12098.

[44] J.R. Jennings, A. Ghicov, L.M. Peter, P. Schmuki, A.B. Walker, J. Am. Chem. Soc. 130 (2008) 13364–13372.

[45] C. Wen, H. Deng, J.Y. Tian, J.M. Zhang, T. Nonferr, Trans. Nonferr. Met. Soc. 16 (2006) s728–s731.

[46] H.H. Wu, L.X. Deng, S.R. Wang, B.L. Zhu, W.P. Huang, S.H. Wu, S.M. Zhang, J. Disper, Sci. Technol. 31 (2010) 1311–1316.

[47] X. Lan, L. Wang, B. Zhang, B. Tian, J. Zhang, Catal. Today 224 (2014) 163–170.

[48] F.B. Li, X.Z. Li, M.F. Hou, Appl. Catal. B: Environ. 48 (2004) 185–194.

[49] M. Uzunova-Bujnova, R. Todorovska, D. Dimitrov, D. Todorovsky, Appl. Surf. Sci. 254 (2008) 7296–7302.

[50] H. Li, J. Zhou, X. Zhang, K. Zhou, S. Qu, J. Wang, X. Lu, J. Weng, B. Feng, J. Mater. Sci.: Mater. Electron 26 (2015) 2571–2578.

[51] J.M. Macak, H. Hildebrand, U. Marten-Jahns, P. Schmuki, J. Electroanal. Chem. 621 (2008) 254–266.
[52] L. Jing, X. Sun, B. Xin, B. Wang, W. Cai, H. Fu, J. Solid State. Chem. 177 (2004) 3375–3382.
[53] H. Cai, X. Chen, Q. Li, B. He, Q. Tang, Appl. Surf. Sci. 284 (2013) 837–842.
[54] K.B. Jaimy, S. Ghosh, W.K. Gopakumar, J. Solid State. Chem. 196 (2012) 465–470.
[55] A.F. Kanta, M. Poelman, A. Decroly, Sol. Energy Mater. Sol. C 133 (2015) 76–81.